Progress of Theoretical Physics, Vol. 97, No. 3, March 1997

Low Energy Reactions of Halo Nuclei in a Three-Body Model

Kazuhiro YABANA

Graduate School of Science and Technology
Niigata University, Niigata 950-21

(Received November 22, 1996)

Low energy nuclear reactions of nuclei with halo structure are theoretically studied in a three-body model in which the projectile is described as the weakly bound state of the halo neutron and core nucleus. A time-dependent wave packet method is employed to solve the three-body Schrödinger equation and to calculate reaction probabilities. Numerical results with various internal Hamiltonians reveal that the reaction mechanisms depend strongly on the single particle structures of the core and target nuclei. The adiabatic dynamics is found to be important when the neutron is bound tightly in the projectile. For a weakly bound projectile with halo structure, the fusion probability is found to decrease due to the addition of a neutron.

§ 1. Introduction

During the last decade, there has been much progress made in the study of light unstable nuclei by experiments with secondary unstable nuclear beams. Near the neutron drip-line, neutron halo structure has been discovered systematically.[1),2)] High energy secondary beam experiments have been useful to extract structure information of the unstable nuclei. Glauber-type theory is useful for the reaction of incident energies higher than a few tens of MeVs.[3)] The reaction experiments have recently been extended to the low incident energy region, close to the Coulomb barrier.[4)]

In the low energy reactions of neutron rich unstable nuclei, dynamical roles of the excess neutrons are expected. Much attention has been paid to the fusion reaction, and in particular to the question of whether the fusion cross section is enhanced in the neutron rich nuclei. As an extreme case, there have been presented several theoretical arguments on the fusion reaction of the nuclei with halo structure.[5)] In these arguments, however, a specific reaction model is usually assumed for the dynamics of the halo neutron during the reaction, and the possible mechanisms which may enhance the fusion probability are discussed. Recently, Kim et al. have studied the transfer and fusion reactions of neutron rich nuclei with the time-dependent Hartree-Fock method.[6)] The coupled-channel calculation has also been done for light system.[7)]

We previously reported the analysis of a three-body model in one spatial dimension which simulates the low energy reactions of halo nuclei.[8)] By exactly solving the three-body Schrödinger equation, we investigated the fusion reactions without any assumptions regarding reaction dynamics. There we found a decrease of the fusion probability by adding the halo neutron to the projectile. In the present paper, we extend our analysis of the three-body model to a realistic three-dimensional three-body system.

The present paper is organized as follows: In § 2, our three-body model is presented. A time-dependent wave packet method to solve the three-body problem is

then presented. In § 3, the calculated results are presented when the neutron is bound tightly in the projectile nucleus. In § 4, the results for the projectile with halo structure are presented. In § 5, concluding remarks are given.

§ 2. Formulation

2.1. *Three-body model*

We consider a nucleus with a single neutron halo, like a ^{11}Be nucleus. The three-body system is composed of the halo neutron and the core nucleus, which constitute the projectile and the target nucleus. We show in Fig. 1 the coordinate system in the incident channel, which will be used in the numerical calculations. The relative coordinate between the neutron and core nucleus is denoted by $\boldsymbol{r}$, and the relative coordinate between the projectile and target nucleus is denoted by $\boldsymbol{R}$. The time-dependent Schrödinger equation for this system is given as

$$i\hbar\frac{\partial}{\partial t}\psi(\boldsymbol{R},\boldsymbol{r},t)=\left\{-\frac{\hbar^2}{2M}\nabla_{\boldsymbol{R}}^2-\frac{\hbar^2}{2\mu}\nabla_{\boldsymbol{r}}^2+V_{cT}(R_{cT})+V_{nc}(r)+V_{nT}(r_{nT})\right\}\psi(\boldsymbol{R},\boldsymbol{r},t)\,. \tag{2·1}$$

In the above equation, M and μ are the reduced masses between the projectile and target nuclei and between the neutron and core nucleus, respectively. R_{cT} and r_{nT} are the distances between the core and target nuclei and between the neutron and target nucleus, respectively. V_{cT}, V_{nc} and V_{nT} are the interaction potentials between the core and target nuclei, neutron and core nucleus, and neutron and target nucleus, respectively.

The neutron potentials V_{nc} and V_{nT} are taken to be real with the standard Woods-Saxon form. The potential between the core and target nuclei, V_{cT}, consists of three terms, the nuclear attractive real potential, the nuclear absorptive imaginary potential, and the Coulomb repulsive potential. They are chosen so that the potential V_{cT} describes the two-body collision of the core and target nuclei, in which the loss of the flux caused by the absorptive potential accounts for the fusion reaction.

In the calculations presented below, we investigate the reaction which simulates the ^{11}Be+^{40}Ca system. For the neutron-core and neutron-target potentials, we choose the radius and the diffuseness parameters of the Woods-Saxon potentials as r_0=1.3 fm and a=0.7 fm. The depths of the potentials are changed and are specified for each calculation. For the core-target potential, we also use the Woods-Saxon form for the nuclear part, $V=-50$ MeV, $W=-10$ MeV, $r_v=1.26$ fm, $r_w=1.215$ fm, $a_v=0.44$ fm, $a_w=0.45$ fm and $R_{v,w}=r_{v,w}(A_c^{1/3}+A_T^{1/3})$. This potential is known to reproduce

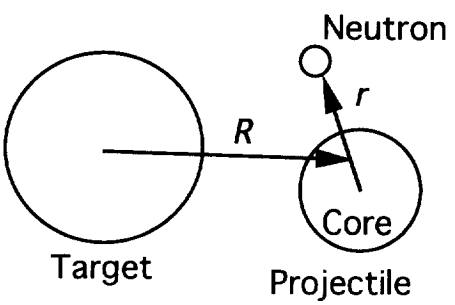

Fig. 1. The three-body system in the model. The incident channel coordinate system which is used in the calculation is shown.

systematically the fusion reactions of light nuclei.[9]

Since the Hamiltonian in Eq. (2·1) is rotationally scalar, the total angular momentum is conserved. Because of the practical limitation of the numerical calculations in our method, we have investigated only the case of total angular momentum $L=0$. We also set the incident relative angular momentum as $l=0$. To understand the mechanism of fusion, the reaction dynamics of this incident channel will be valuable.

2.2. *Time-dependent method*

Although the three-body Hamiltonian in Eq. (2·1) is static, we develop a numerical method in which we first solve the time-dependent Schrödinger equation for an initial incoming wave packet. Static scattering information will then be extracted from the final outgoing wave packet by a method of energy projection.

The method will be presented for the case of zero total angular momentum. We take polar coordinate systems for both $\boldsymbol{R}$ and $\boldsymbol{r}$. The wave function can be expressed as

$$\psi_{L=0}(\boldsymbol{R}, \boldsymbol{r}, t)=\sum_{l=0}^{\infty}\frac{u_l(R, r, t)}{Rr}\sum_{m=-l}^{l}Y_{lm}(\hat{R})\,Y_{lm}^{*}(\hat{r})\,. \tag{2·2}$$

The angular part of the wave function can be expressed by the Legendre function $P_l(\cos\theta)$, in which the angle θ is that between $\boldsymbol{R}$ and $\boldsymbol{r}$. The Schrödinger equation for the radial wave function is given by

$$\begin{aligned} &i\hbar\frac{\partial}{\partial t}u_l(R, r, t)\\ &=\left\{-\frac{\hbar^2}{2M}\frac{d^2}{dR^2}+\frac{\hbar^2 l(l+1)}{2MR^2}-\frac{\hbar^2}{2\mu}\frac{d^2}{dr^2}+\frac{\hbar^2 l(l+1)}{2\mu r^2}+V_{nc}(r)\right\}u_l(R, r, t)\\ &\quad+\sum_{l'}V_{ll'}(R, r)\frac{2l'+1}{2}u_{l'}(R, r, t)\,, \end{aligned} \tag{2·3}$$

with the potential $V_{ll'}(R, r)$ defined by

$$V_{ll'}(R, r)=\int d(\cos\theta)P_l(\cos\theta)P_{l'}(\cos\theta)\{V_{cT}(R_{cT})+V_{nT}(r_{nT})\}\,. \tag{2·4}$$

For the initial conditions, the neutron orbital is set to the $2s$ bound orbital of the neutron-core potential and is denoted as $\phi_0(r)$. For the relative motion between the projectile and target nuclei, we employ the wave packet state which satisfies the following conditions: the wave packet consists only of the incoming waves in the incident $l=0$ channel, and it is confined in a finite radial region in which only the Coulomb part of the core-target potential exists. In practice we use the following Gaussian wave packet:

$$u_l(R, r, t_0)=\delta_{l0}\left(\frac{2\gamma}{\pi}\right)^{3/4}\exp[-\gamma(R-R_0)^2-iK_0R]\phi_0(r)\,. \tag{2·5}$$

We solve Eq. (2·3) by discretizing both time and radial variables. The wave function after a short time period Δt is obtained by applying the following two

procedures to the previous wave function. First the time evolution by a part of the Hamiltonian which is diagonal in the angular momentum space is considered:

$$h_l = h_l^{(R)} + h_l^{(r)}, \tag{2·6}$$

$$h_l^{(R)} = -\frac{\hbar^2}{2M}\frac{d^2}{dR^2} + \frac{\hbar^2 l(l+1)}{2MR^2} + V_{CT}(R), \tag{2·7}$$

$$h_l^{(r)} = -\frac{\hbar^2}{2\mu}\frac{d^2}{dr^2} + \frac{\hbar^2 l(l+1)}{2\mu r^2} + V_{nC}(r). \tag{2·8}$$

Each partial wave function is then considered as evolving in time according to the Crank-Nicholson formula,[10]

$$u_l^{(n+(1/2))} = \frac{1-\frac{i\Delta t}{2\hbar}h_l^{(r)}}{1+\frac{i\Delta t}{2\hbar}h_l^{(r)}} \frac{1-\frac{i\Delta t}{2\hbar}h_l^{(R)}}{1+\frac{i\Delta t}{2\hbar}h_l^{(R)}} u_l^{(n)}. \tag{2·9}$$

Next, the potential which mixes the different partial waves is applied,

$$u_l^{(n+1)} = u_l^{(n+(1/2))} - \frac{i\Delta t}{\hbar}\sum_{l'}\Delta V_{ll'}(R, r)\frac{2l'+1}{2}u_{l'}^{(n+(1/2))}, \tag{2·10}$$

where $\Delta V_{ll'}$ is defined as $\Delta V_{ll'}(R, r) = V_{ll'}(R, r) - \delta_{ll'} V_{CT}(R)$.

We employ a radial mesh size 0.5 fm for both R and r up to 40 fm. The five point formula is employed in approximating the second order differential operator. To describe accurately the transfer processes within the incident channel coordinate system, it is necessary to include partial waves of large l value. We included up to $l=60$, and confirmed the convergence of the results. The total number of mesh points to describe the wave function in each time step is, thus, approximately $N=80\times80\times60$.

Initially the center of mass of the wave packet is located at $R_0=22$ fm with the width of $\gamma=0.05$ fm^{-2} in Eq. (2·5). The time integration is continued until the center of mass of the final wave packet, which consists only of the outgoing waves, is located at around 20 fm. About 1000 time steps are employed for the time evolution. More time steps are required to obtain convergent results when the reaction probabilities (especially transfer probabilities) have a strong energy dependence.

We show in Fig. 2 a typical density profile of the wave packet in the calculation. The density integrated over the angle θ_{Rr} is plotted in the R,r plane,

$$\rho(R, r) = R^2 r^2 \int d\hat{R} d\hat{r} \, |\psi(\boldsymbol{R}, \boldsymbol{r}, t)|^2. \tag{2·11}$$

In the initial density shown in Fig. 2(a), the nodal structure in the $2s$ neutron wave function is seen in the r direction. The wave packet moves toward negative R direction. There is a Coulomb barrier around the $R\sim10$ fm region. A component which penetrates the barrier is absorbed by the core-target potential, which represents the fusion reaction. The final wave packet in Fig. 2(b) consists of two parts, the elastic and inelastic parts, which are confined in the small r region, and the transfer part which is located around the $R\sim r$ region. Both waves move in the positive R

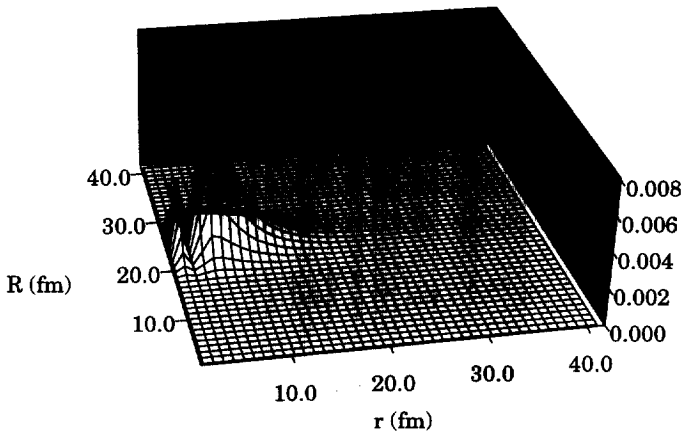

(a)

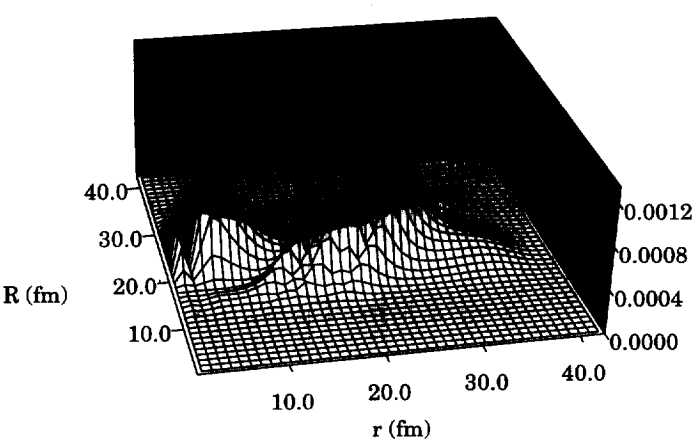

(b)

Fig. 2. Radial density distribution of the time-dependent wave packet integrated over angle variables. The initial wave packet is depicted in (a) and the final wave packet in (b).

direction. In the figure, the breakup probability is small and is not seen.

2.3. *Energy projection*

A wave packet solution includes scattering information for a certain incident energy region. To extract the scattering information of a fixed incident energy E, we first define the energy distribution function of the wave packet,

$$W_a(E)=\langle\psi_a|\delta(E-\hat{H})|\psi_a\rangle\,, \tag{2·12}$$

where $\hat{H}$ represents the total three-body Hamiltonian. Employing the Fourier transform of the δ-function, the energy distribution function can be expressed as

$$W_a(E)=\frac{1}{\pi\hbar}\mathrm{Re}\int_0^{+\infty}dt e^{iEt/\hbar}\left\langle\psi_a\left(-\frac{t}{2}\right)\middle|\psi_a\left(\frac{t}{2}\right)\right\rangle\,. \tag{2·13}$$

The wave function $\psi_a(t)$ satisfies the Schrödinger equation (2·1) with the initial condition $\psi_a(0)=\psi_a$. Thus the method to solve Eq. (2·1) can again be used to obtain the energy distribution functions.

Since the imaginary potential is included only in the core-target potential, a loss of flux in the three-body calculation represents fusion between the core and target nuclei. We regard the loss of flux as fusion in the three-body reaction, irrespective of the destination of the halo neutron. The present definition of fusion, therefore, includes both complete and incomplete (one neutron escaping) fusion.

The fusion probability at energy E, $P_f(E)$, is defined as the ratio of the loss of the energy distribution to the initial energy distribution,

$$P_f(E)=\frac{W_i(E)-W_f(E)}{W_i(E)}\,, \tag{2·14}$$

where $W_{i(f)}(E)$ are the energy distribution functions calculated with the initial (final) wave packets, respectively.

We next discuss the method to extract the probabilities of the elastic, inelastic and transfer processes. For elastic scattering, we define the elastic distribution function

$$W_f^{\mathrm{el}}(E)=\int d\boldsymbol{K}\delta\left(\frac{\hbar^2K^2}{2M}+\epsilon_0-E\right)|\langle\psi_{\boldsymbol{K}}(\boldsymbol{R})\phi_0(r)|\psi(\boldsymbol{R},\boldsymbol{r},t_f)\rangle|^2\,, \tag{2·15}$$

where ϵ_0 is the binding energy of the neutron in the core nucleus, and $\psi_{\boldsymbol{K}}(\boldsymbol{R})$ is a regular Coulomb wave function with the incident wave number vector $\boldsymbol{K}$. The elastic scattering probability is calculated as

$$P_{\mathrm{el}}(E)=\frac{W_f^{\mathrm{el}}(E)}{W_i(E)}\,. \tag{2·16}$$

Similarly, the probabilities for the inelastic reactions can be calculated. To obtain the transfer probability, the transfer distribution function,

$$W_f^{\mathrm{tr}(i)}(E)=\int d\boldsymbol{K}\delta\left(\frac{\hbar^2K^2}{2M_T}+\epsilon_i-E\right)|\langle\psi_{\boldsymbol{K}}(\boldsymbol{R}_T)\phi_i(r_{nT})|\psi(\boldsymbol{R},\boldsymbol{r},t_f)\rangle|^2\,, \tag{2·17}$$

must be calculated. Here M_T and $\boldsymbol{R}_T$ are the reduced mass and the relative coordinate of the motion between the core nucleus and the target nucleus with transferred neutron. $\phi_i(r_{nT})$ is the i-th bound orbital of the neutron-target system, whose binding energy is given by ϵ_i. The function $\psi_K(\boldsymbol{R}_T)$ again represents the regular Coulomb wave function. The transfer probability for the i-th target orbital is calculated as

$$P_{\mathrm{tr}(i)}(E)=\frac{W_f^{\mathrm{tr}(i)}(E)}{W_i(E)}. \tag{2·18}$$

We denote the inelastic and transfer probabilities summed over the orbitals as $P_{\mathrm{tr}}(E)$ and $P_{\mathrm{inel}}(E)$, respectively. In evaluating Eq. (2·15), two-dimensional numerical integration over R and r is necessary. For Eq. (2·17), the three-dimensional integration over R, r and θ_{Rr} as well as the sum over l is necessary.

Finally, the breakup probability is calculated as the remainder:

$$P_{\mathrm{bu}}(E)=1-P_f(E)-P_{\mathrm{el}}(E)-P_{\mathrm{inel}}(E)-P_{\mathrm{tr}}(E). \tag{2·19}$$

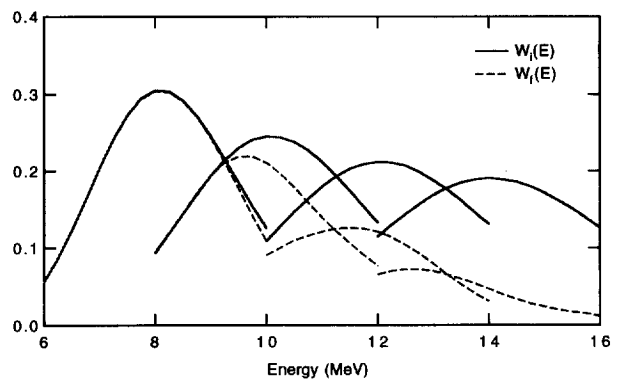

(a)

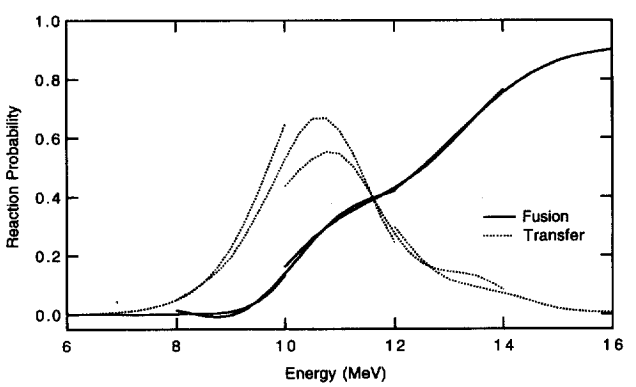

(b)

Fig. 3. (a) Energy distribution for the four wave packets with different average energies. Solid curves are for initial wave packets and dashed curves for final wave packets. (b) Fusion (solid) and transfer (dotted) probabilities calculated with the four different wave packets are compared.

The reaction probabilities calculated in the above prescription should not depend on the initial wave packet. We show the comparison of the reaction probabilities with different initial wave packets in Fig. 3. In Fig. 3(a), the energy distribution functions which are calculated with four different initial wave packets with average energies of 8, 10, 12 and 14 MeV are shown. The solid and dashed curves are the energy distributions calculated with the initial and final wave packets, respectively. The fusion probability is calculated according to Eq. (2·14) and is shown by the solid curves in Fig. 3(b). The curves calculated with different wave packets are seen to overlap with good accuracy. The transfer probabilities calculated with different wave packets are also shown by the dashed curves in Fig. 3(b). The transfer probabilities show strong energy dependence, and are slightly less accurate. In displaying the energy dependence of the reaction probabilities below, we performed the calculations with four initial wave packets with average incident energies of 8, 10, 12, 14 MeV. These values are then connected at 9, 11, 13 MeV.

§ 3. Tightly bound projectile

In this section, we investigate the reaction mechanisms when the neutron is bound rather tightly in the projectile. We set the neutron-core potential depth to -65 MeV. The neutron occupies the $2s$ orbital, whose binding energy ϵ_0 is -3.58 MeV.

To elucidate the reaction mechanism, and in particular the role of the neutron in the fusion reaction, we first show reaction probabilities varying the depth of the neutron-target potential. The projectile incident energy is fixed at 12 MeV, which is close to the energy of the Coulomb barrier top.

In Fig. 4, the reaction probabilities of the fusion, inelastic, transfer and breakup processes are plotted against the depth of the neutron-target potential V_T. The fusion probability of the core-target collision without neutron is 0.37 at the present incident energy. The fusion probability exhibits oscillatory behavior as a function of V_T. On average, the fusion probability is slightly larger than that without the neutron. The inelastic and transfer probabilities are the values summed over the single particle orbitals which the neutron ultimately occupies. In practice, only one or two orbitals of small binding energies are occupied by the neutron in the inelastic and transfer processes. Therefore, the Pauli exclusion principle, which we do not take into account in the present calculation, should not be important. The transfer

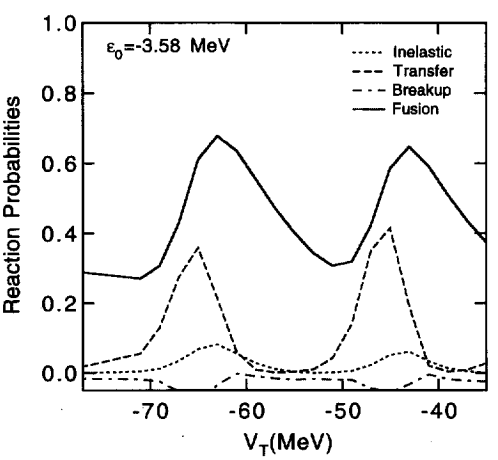

Fig. 4. Fusion (solid), inelastic (short dashed), transfer (long dashed) and breakup (long-short dashed) probabilities are shown against the depth of neutron-target potential. The neutron is bound tightly in the projectile before collision.

probability shows significant dependence on V_T, and is correlated with the V_T dependence of the fusion probability. The breakup probability is small and even negative in some region of V_T. As noted in the previous section, we calculate the breakup probability as the remainder of the probabilities of the fusion, elastic, inelastic and transfer processes, which are calculated independently. Therefore, the numerical errors are accumulated in the breakup probability and even result in a small negative value.

In the V_T region of large transfer probability, the binding energy of the single particle orbital in the target nucleus with large transfer probability is close to that in the projectile. The target orbitals are the $2p$ state around $V_T=-45$ MeV, and the $3s$ state around $V_T=-65$ MeV.

The strong influence of the single particle orbitals of the target nuclei on the fusion and transfer probabilities indicates the importance of the adiabatic dynamics. Namely, the static neutron orbitals which extend to both core and target nucleus are formed. The oscillation of the fusion probability in changing the neutron-target potential depth may be understood as follows. When the neutron-target potential has a bound state whose binding energy is slightly smaller than the binding energy of the initial neutron orbital in the projectile nucleus, the single particle energy of the initial neutron orbital will be pushed down by the interaction with the target potential, as can be understood using the two-level perturbation theory. The increase of the binding energy in the projectile causes an increase of the kinetic energy of the projectile-target relative motion, and thus results in an increase of the fusion probability. An opposite mechanism works when the neutron state in the target potential is slightly more deeply bound than the initial neutron state in the projectile. When the orbitals of the core and target potential are approximately degenerate, the occurrence of the strong mixing of the two orbitals results in a large transfer probability.

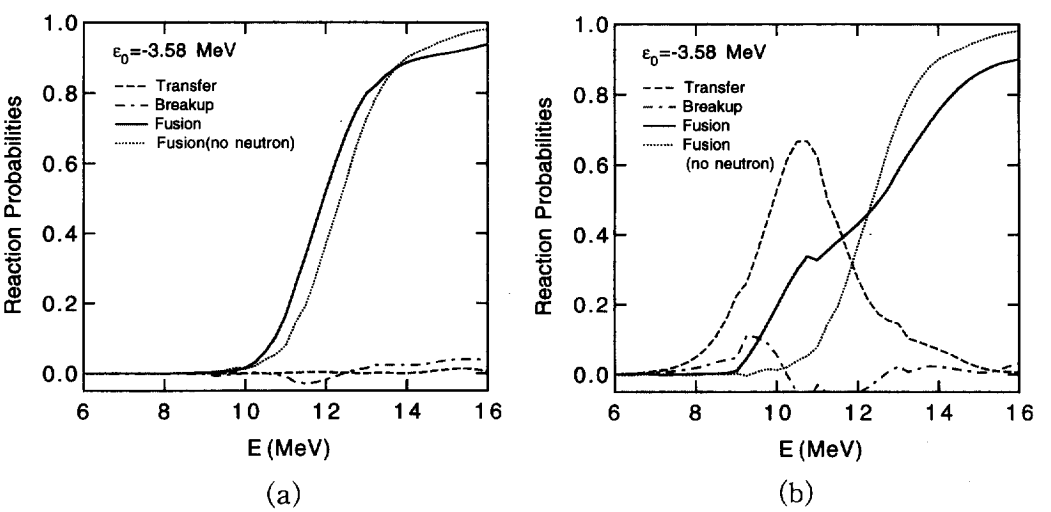

Fig. 5. Incident energy dependence of various reaction probabilities when (a) the transfer probability is small ($V_T=-58$ MeV) and (b) the transfer probability is large ($V_T=-67$ MeV). The neutron is bound tightly in the projectile before collision.

We next show the incident energy dependence of the reaction probabilities, fixing the neutron-target potential depth. We choose two V_T values, $V_T=-58$ MeV in Fig. 5(a), where the transfer probability is small, and $V_T=-67$ MeV in Fig. 5(b), where the large transfer probability is seen. In both figures, the fusion and transfer probabilities are shown. The core-target fusion probability without neutron is also shown for comparison.

Figure 5(a) indicates that the influence of the neutron on the fusion probability is to shift the incident energy dependence. Namely, the addition of the neutron changes the fusion barrier height by a constant amount. This is consistent with our picture of the adiabatic dynamics. Since the formation of the adiabatic neutron orbital depends on the relative distance between two nuclei and does not depend on the relative velocity, the shift of the barrier height is independent of the incident energy.

The energy dependence is different in Fig. 5(b), where a large transfer probability is seen. The transfer probability here has a maximum in the incident energy slightly below the barrier top. The fusion probability in this case is larger than that without the neutron when the incident energy is low and smaller when the incident energy is high. Thus the fusion barrier has a strong incident energy dependence.

The calculated energy dependence of the fusion probability resembles those which have been observed in subbarrier fusion enhancement phenomena. One way to understand the relation between the energy dependences of the transfer and fusion probabilities may be given by the dispersion relation of the optical potential for elastic scattering. Let us suppose to construct an optical potential which describes elastic scattering of the present three-body model. The imaginary part of the optical potential should have a strong absorptive component caused by the large transfer probability, in addition to the absorptive core-target potential. A rapid increase of the transfer probability causes an increase of the absorptive potential as a function of the incident energy. Due to the dispersion relation which connects the real and imaginary parts of the optical potential, the real part of the optical potential should also have an incident energy dependence and cause the energy dependence of the fusion barrier.[11]

§ 4. Weakly bound projectile (halo nuclei)

We choose a neutron-core potential depth of -53 MeV, in which the binding energy of the neutron in the projectile is small, 0.61 MeV, in the $2s$ orbital. The wave function exhibits a spatially extended halo structure. Close to this parametrization but with the spin-orbit interaction, we presented the *B(E1)* distribution of ^{11}Be nucleus as a function of excitation energy, and found that the measured strong *B(E1)* strength is reasonably reproduced.[12] Since we exactly solve the three-body Schrödinger equation, our calculation includes the effect of the strong *B(E1)* strength in the low excitation.

In Fig. 6, the reaction probabilities changing the neutron-target potential depth is shown. The incident energy is fixed at 12 MeV, as in the previous section. The most significant feature is the decrease of the fusion probability by adding a halo neutron. The fusion probability in the three-body model is smaller than the value without the

neutron, 0.37, for almost all regions of V_T values. There is oscillatory behavior seen in the fusion and transfer probabilities. We thus suppose the adiabatic dynamics is still important in the weakly bound projectile, though the amplitude of the oscillation is smaller than that in the tightly bound case. In the present case, the breakup probability is also substantial. The energy region with large breakup probability correlates with that with large transfer probability.

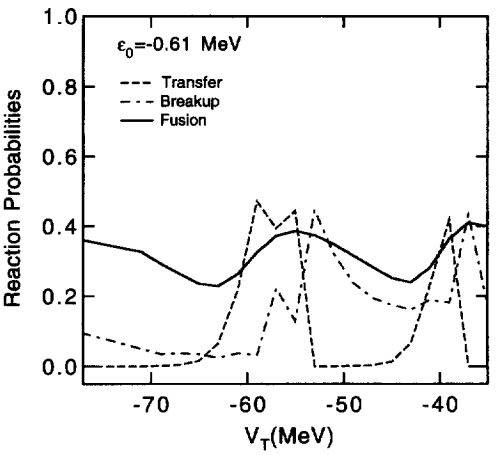

Fig. 6. Various reaction probabilities against the depth of neutron-target potential. The neutron is bound weakly in the projectile before collision.

The reason for the decrease of the fusion probability in the case of the weakly bound projectile may be understood as follows.*) When the neutron orbital in the target nucleus is bound slightly deeper than the weakly bound projectile orbital, the fusion probability will decrease due to the coupling between two orbitals, as in the case of the tightly bound projectile. However, since the neutron is bound very weakly, the opposite situation cannot take place. Therefore, only the decrease in the fusion is seen when changing V_T values.

Another possible reason for the decrease of the fusion would be a neutron spectator picture, which we proposed in our previous analysis in the one-dimensional model.[8] In the limit of the weak binding of the halo neutron, the influence of the halo neutron on the fusion reaction between the core and target nuclei would be negligible. The fusion reaction then proceeds essentially in the two-body collision of the core and target nuclei. However, the incident energy of the projectile is shared between the halo neutron and the core nucleus. Therefore, the effective incident energy of the core nucleus is smaller by the amount $\Delta E = m_n/(M_C + m_n)E_{\text{inc}}$.

The shift of the incident energy in the present mechanism is about 1 MeV. The fusion probability at the shifted energy (11 MeV) without the neutron is about 0.1. This fact indicates that, though the spectator mechanism of the halo neutron could explain the decrease of fusion probability, the neutron binding in the present model is not so weak that the neutron spectator picture does not work quantitatively.

As in the tightly bound case, the transfer probability is large when there is a neutron orbital in the neutron-target system whose binding energy is nearly degenerate with the initial neutron orbital in the core nucleus. Since the halo neutron is bound very weakly, the target bound states of approximate degeneracy are also bound weakly. At a slightly shallower neutron-target potential, the target neutron states become unbound. The large breakup probability accompanying the abrupt decrease of the transfer probability with decrease in the depth of the neutron-target potential is seen in the figure and can be understood as the transfer to the target unbound

*) The author is grateful to one of the referees who kindly pointed out the reason explained in the present paragraph.

orbitals. For each peak of the transfer probability, the relevant neutron orbitals of the target nuclei are the $2p$ orbital at $V_T=-40$ MeV, $3s$ orbital at $V_T=-55$ MeV, and $2d$ orbital at $V_T=-60$ MeV.

For the reaction of the halo nuclei, the role of the *B(E1)* strength at low excitation has been studied.[5] The breakup processes by way of such excitation are also expected in the present calculation, including the Coulomb excitation caused by the core-target Coulomb potential. In the present calculation, however, the dominant process contributing to the breakup is the quasi-bound orbital of the target potential, as mentioned above. The breakup process by way of the dipole excitation of the projectile should not be sensitive to the target potential depth. In the calculation, the breakup probability is rather small in the V_T region of -60 to -70 MeV. This indicates that the breakup process by way of the dipole excitation of the projectile is not an important process in the present model.

In Figs. 7(a)~(c), we show the incident energy dependence of the reaction

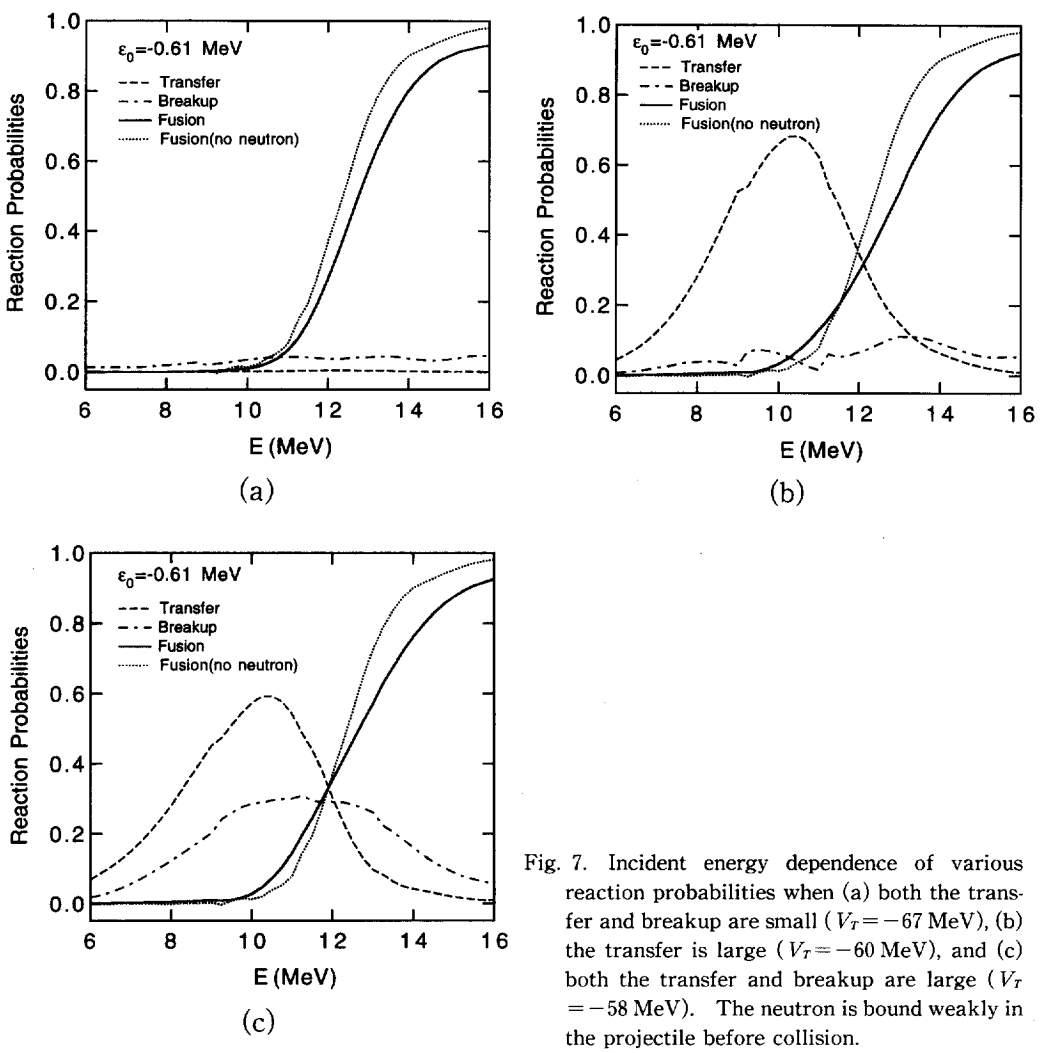

Fig. 7. Incident energy dependence of various reaction probabilities when (a) both the transfer and breakup are small ($V_T=-67$ MeV), (b) the transfer is large ($V_T=-60$ MeV), and (c) both the transfer and breakup are large ($V_T=-58$ MeV). The neutron is bound weakly in the projectile before collision.

probabilities. The V_T value is set to -67 MeV in (a), where the transfer and breakup probabilities are small, to -60 MeV in (b), where the transfer probability is large but with small breakup, and to -58 MeV in (c), where both the transfer and breakup probabilities are substantial. In each figure, the core-target fusion probability without the neutron is shown as a reference.

When both the transfer and breakup probabilities are small (Fig. 7(a)), the energy dependence of the fusion probability is similar to that without neutron. The fusion probability is smaller by an approximately constant amount, though a slight energy dependence of the fusion barrier is seen. When a large transfer occurs (Fig. 7(b)), the fusion barrier shows an energy dependence as in the tightly bound case (Fig. 5(b)). Though the fusion probability is slightly enhanced at low incident energy, it is reduced near barrier and at higher incident energies. In the transfer process, the halo neutron is transferred to $3s$ and $2d$ target orbitals. Figure 7(c) is calculated with a slightly shallower V_T value than Fig. 7(b), and the $2d$ orbital is now unbound. The fusion probability is very similar to the case of Fig. 7(b). The transfer process to the $2d$ orbital in Fig. 7(b) becomes the breakup in Fig. 7(c). Comparing with the transfer reaction of the tightly bound case, the transfer probability extends to the lower incident energy in the weakly bound case. The halo wave function extends in a large spatial region so that the transfer process may take place even when the two nuclei do not come close in the low incident energy.

§ 5. Concluding remarks

We presented an analysis of the three-body model to investigate the reaction mechanisms of the low energy reactions of halo nuclei.

We presented a method to solve the three-body scattering problem in which the time-dependent Schrödinger equation is solved for the incoming wave packet state. We then explained a way to extract reaction probabilities for a fixed incident energy from the final outgoing wave packet. Though the time dependent method used provides an intuitive view of the reaction, it requires large computer resources. We achieved the calculation of zero total angular momentum only.

When the neutron is bound tightly in the projectile, the adiabatic dynamics are found to be important. The attractive neutron-target potential does not always increase the fusion probability. Instead, the neutron-target potential influences the fusion barrier either attractively or repulsively, depending on the relative single particle energies of the neutron orbitals in the core and the target nuclei around the Fermi level. When the neutron orbitals of the core and the target nuclei are approximately degenerate, a large transfer probability is seen. The fusion barrier height also shows a strong energy dependence in this case.

When the neutron is bound weakly and exhibits halo structure, the fusion probability is found to decrease with the addition of the halo neutron. This may be understood as follows: Since the neutron is bound weakly in the projectile, the neutron orbital in the target nucleus is usually bound deeper than that of the projectile. Therefore, only the repulsive effect for the fusion barrier emerges by the coupling of two orbitals. As another possible reason, we also propose the neutron spectator

picture in which the decrease of the effective incident energy of the core nucleus results in a repulsive effect on the fusion barrier.

Acknowledgements

This work is supported by the Grant in Aid for Scientific Research (No. 08740197) of the Ministry of Education, Science and Culture (Japan). Numerical calculations were performed on the FACOM VPP-500 supercomputer in RIKEN.

References

1) I. Tanihata et al., Phys. Lett. **B160** (1985), 380.
I. Tanihata et al., Phys. Rev. Lett. **55** (1985), 2676.
I. Tanihata et al., Phys. Lett. **B206** (1988), 592.
2) K. Ikeda, Nucl. Phys. **A538** (1992), 355c.
P. G. Hansen and B. Jonson, Europhys. Lett. **4** (1987), 409.
3) G. F. Bertsch, B. A. Brown and H. Sagawa, Phys. Rev. **C39** (1989), 1154.
Y. Ogawa, K. Yabana and Y. Suzuki, Nucl. Phys. **A543** (1992), 722.
K. Yabana, Y. Ogawa and Y. Suzuki, Nucl. Phys. **A539** (1992), 295; Phys. Rev. **C45** (1992), 2909.
4) A. Yoshida et al., Nucl. Phys. **A588** (1995), 99c.
5) N. Takigawa and H. Sagawa, Phys. Lett. **B265** (1991), 23.
M. S. Hussein et al., Phys. Rev. **C46** (1992), 377.
C. A. Bertulani and A. B. Balantekin, Phys. Lett. **B314** (1993), 275.
C. H. Dasso and A. Vitturi, Phys. Rev. **C50** (1994), R12.
6) K. -H. Kim, T. Otsuka and M. Tohyama, Phys. Rev. **C50** (1994), R566.
7) B. Imanishi and W. von Oertzen, Phys. Rev. **C52** (1996), 3249.
8) K. Yabana and Y. Suzuki, Nucl. Phys. **A588** (1995), 99c.
9) D. M. Brink, *Semi-Classical Methods in Nucleus-Nucleus Scattering* (Cambridge University Press, 1985).
10) S. E. Koonin, *Computational Physics*, Chap. 7 (The Benjamin/Cummings Publishing Company, 1985).
11) M. A. Nagarajan, C. C. Mahaux and G. R. Satchler, Phys. Rev. Lett. **54** (1985), 1136.
C. Mahaux, H. Ngo and G. R. Satchler, Nucl. Phys. **A449** (1986), 354.
12) T. Kido, K. Yabana and Y. Suzuki, Phys. Rev. **C53** (1996), 2296.